Hydrol. Earth Syst. Sci. Discuss., 10, 5799–5830, 2013
www.hydrol-earth-syst-sci-discuss.net/10/5799/2013/
doi:10.5194/hessd-10-5799-2013

Hydrology and Earth System Sciences
Open Access
Discussions

Hydrological modelling of a slope covered with shallow pyroclastic deposits from field monitoring data

R. Greco[1], L. Comegna[1], E. Damiano[1], A. Guida[1,2], L. Olivares[1], and L. Picarelli[1]

[1]Dipartimento di Ingegneria Civile Design Edilizia e Ambiente, Seconda Università di Napoli, via Roma 29, 81031 Aversa (CE), Italy
[2]Centro Euro-Mediterraneo sui Cambiamenti Climatici, via Maiorise, Capua (CE) 81043, Italy

Received: 24 April 2013 – Accepted: 29 April 2013 – Published: 7 May 2013

Correspondence to: R. Greco (roberto.greco@unina2.it)

Published by Copernicus Publications on behalf of the European Geosciences Union.

Abstract

A one-dimensional hydrological model of a slope covered with pyroclastic materials is proposed. The soil cover is constituted by layers of loose volcanic ashes and pumices, with a total thickness of around 2.40 m, laying upon a fractured limestone bedrock. The inclination of the slope is around 40°, slightly larger than the friction angle of the ashes. Thus, the equilibrium of the slope, significantly affected by the cohesive contribution exerted by soil suction in unsaturated conditions, may be altered by rainfall infiltration. The model assumes a single homogeneous soil layer occupying the entire depth of the cover, and takes into account seasonally variable canopy interception of precipitation and root water uptake by vegetation, mainly constituted by deciduous chestnut woods with a dense understory growing during late spring and summer. The bottom boundary condition links water potential at the soil-bedrock interface with the fluctuations of the water table of the aquifer located in the fractured limestone, which is simply modelled as a linear reservoir. Most of the model parameters have been assigned according to literature indications or from experimental data, and only a few have been identified by means of calibration against the water potential data measured at a monitoring station along the slope between 1 January 2011 and 20 July 2011. The calibrated model, which reproduced very closely the data of the calibration set, has been applied to the simulation of the hydrological response of the slope to the hourly precipitation record of 1999, when a large flowslide was triggered not far from the monitored location. The simulation results show that the minimum soil suction ever attained occurred just at the time the flowslide was triggered, indicating that the model is capable of correctly predicting the potential establishment of slope failure conditions.

HESSD
10, 5799–5830, 2013

1 Introduction

Large areas of the Apennines of Campania (Southern Italy) are characterised by slopes covered with few meters of loose pyroclastic deposits laying upon a fractured carbonate bedrock, in which often karst aquifers are located, drained by either perennial or temporary springs (Celico et al., 2006; Petrella et al., 2007, 2009). The equilibrium of such deposits is strongly affected by pore water pressure: in gentle slopes, with inclination smaller than the internal friction angle of the soil constituting the deposit, φ', the increment of positive pore water pressure causes the reduction of the effective stress, which may lead to the failure of the slope; in steep slopes, with inclination comparable or higher than φ', the equilibrium is possible in unsaturated conditions, thanks to the cohesive action between particles exerted by soil suction, which, after soil wetting, may drop until the triggering of a landslide.

Shallow landslides involving the pyroclastic covers of the slopes of the Apennines of Campania are extremely fast and sudden, and usually not preceded by warning signs, such as small movements and/or formation of cracks. These features make them among the most worrisome and unpredictable natural hazards.

Clearly, rainfall is the main cause of such landslides, but the actual achievement of the triggering conditions is strongly influenced by other concurring factors, such as stratigraphical (Crosta and Dal Negro, 2003) or geometrical discontinuities, i.e. road cuts or scarps (Guadagno et al., 2005), and flow concentration caused by slope or bedrock morphology, or by springs at the soil-bedrock interface (Cascini et al., 2008). Furthermore, also the vegetation cover plays an important role in the hydrological balance of a slope: root water uptake deeply affects water movement through the unsaturated zone of soil (Feddes et al., 1976), and canopy is capable of intercepting a significant amount of precipitation (Muyzlo et al., 2009).

The development of hydrological models of slope response to precipitations, coupled with slope equilibrium models allowing the safety factor to be evaluated (Montgomery and Dietrich, 1994; Rosso et al., 2006; Capparelli and Versace, 2010; Arnone et al.,

HESSD
10, 5799–5830, 2013

2011; Netti et al., 2012), is a key point for setting up effective early warning systems, which represent the most promising approach for the mitigation of the resulting diffuse risk. However, still few examples exist of hydrological models used for landslide prediction accounting for the vegetation effects (Ivanov et al., 2008a,b; Nyambayo and Potts, 2010).

Nonetheless, owing to the complexity of the involved hydrological processes and to the scarce availability of monitoring data of natural slopes, empirical criteria for assessing rainfall thresholds are still the most used means to landslide risk management (Versace et al., 2003; Guzzetti et al., 2007).

In this paper, a mathematical model of the hydrological behaviour of the slope of Cervinara, northern of Naples, covered with loose volcanic ashes laying upon fractured limestone is proposed. The model, which has been developed on the basis of the data of an automatic monitoring station operating at the slope since 2009, takes into account, in a simplified way, the hydraulic properties of the unsaturated deposit, the effects of the vegetation cover upon the hydraulic conditions of the top soil, and the hydraulic constraint exerted, at the bottom of the soil cover, by the aquifer located within the fractured bedrock. The proposed model allows reproducing soil suction and water content, observed at various depths in the pyroclastic cover, during the rainy season (from autumn till early spring), as well as during the dryer and warmer season (from late spring till the end of summer).

2 Field monitoring at the slope of Cervinara

The experimental site is located along the northeast slope of Mount Cornito, near the town of Cervinara, about 50 km northwest of Naples, southern Italy, just besides the location where, in the night between 15 and 16 December 1999, a flowslide was triggered after an intense rain event lasting more than 24 h (Olivares and Picarelli, 2001).

The slope, at an elevation between 550 m and 760 m above the sea level, has an average inclination of 40°, and the pyroclastic cover, with a nearly constant thickness

HESSD
10, 5799–5830, 2013

of around 2.5 m, consists of an alternation of loose volcanic ashes, with porosity ranging between 0.70 and 0.75, and pumices laying upon a fractured limestone bedrock. The typical layered soil cover observed along the slope is given in Fig. 1. Such layered profile is the result of the deposition of materials originated by several eruptions of the two main volcanic complexes of Campania (the Somma–Vesuvius and the Phlegrean Fields) occurred during the last 40 000 yr (Rolandi et al., 2003; Di Crescenzo and Santo, 2005). Visual inspection by trenches showed that roots are found within the entire soil depth, with a maximum density in the upper 0.40 m, becoming sparse below 1.50 m depth.

The slope is covered with woods, mainly deciduous chestnuts (*Castanea sativa*) with few deciduous beeches (*Fagus sylvatica*). From May to late September, when the foliage of the trees is present, a dense understory grows, mainly formed by ferns (*Pteridium aquilinum*) and other seasonal shrubs. Few areas at the upper part of the slope are not covered with woods and the vegetation consists of shrubs (*Cytisus scoparius*) and grass (*Festuco Brometea*).

In August 2009 an automatic hydrological monitoring station at high temporal resolution has been installed. Since then, measurements of volumetric water content by Time Domain Reflectometry (TDR) and capillary tension by jet-fill tensiometers have been acquired every two hours. In addition, a rain gauge for hourly automatic acquisition has been installed, with sensitivity to rainfall height increments of 0.2 mm. The monitoring station includes eight tensiometers and seven TDR metallic probes, placed at various depths between 0.60 m and 1.60 m, grouped into two nests of sensors located 5 m apart from each other.

The TDR probes, of various lengths between 10 cm and 40 cm, are connected through coaxial cables and a multiplexer to a Campbell Scientific Inc. TDR-100 reflectometer. Some of the probes are placed in the immediate proximity of the ceramic tips of the tensiometers, so to allow coupling water content and capillary tension measured at the same depths.

HESSD
10, 5799–5830, 2013

The TDR measurements are carried out by means of a specific calibration relationship, linking soil water content with bulk dielectric permittivity, which has been experimentally determined over undisturbed samples of the investigated soil (Greco et al., 2010). The obtained relationship results close to analogous relationships found in literature for similar volcanic soils (Regalado et al., 2003).

For the automatic acquisition and storage of the monitoring data, all the installed equipments are connected to a Campbell Scientific Inc. CR-1000 data logger, and are powered by a 12 V battery connected to a solar panel. A sketch of the entire monitoring station is given in Fig. 2.

Figure 3 shows soil suction and volumetric water content measured at four depths between 1 January 2011 and 20 July 2011, together with the corresponding daily hyetograph. The observed soil suction and water content trends look similar to those observed during the same period in other years. It looks clear that, although after the heaviest rainfall events occurred during winter and early spring, soil suction, especially at the shallowest tensiometer, dropped down to less than 2.0 kPa, the soil was always far from saturation, as indicated by the water content, rarely exceeding 0.40. During late spring and summer, soil suction increased at all depths. Such increment does not seem to be caused by upward evapotranspiration fluxes. In fact, the two deepest tensiometers measured the steepest increasing trend of suction (Fig. 3), and the two upper TDR probes, buried at −0.30 m and −0.60 m, showed a decreasing trend of water content higher than the others (the volumetric water content at those depths dropped from 0.33 to 0.13 and from 0.26 to 0.08 between 1 May 2011 and 20 July 2011, respectively).

Conversely, the summer drainage of the soil cover is likely related with the decrease of the water level in the underlying aquifer located in the fractured bedrock, as it has been reported to occur typically in similar contexts during the dry season (Petrella et al., 2007, 2009). Such interpretation is confirmed by Fig. 4, in which the vertical water potential gradients, observed at three depths during the same period, are plotted. The gradients have been obtained by the differences between the water potential provided by the suction measured by tensiometers buried at adjacent depths. The estimated

HESSD
10, 5799–5830, 2013

gradients resulted always > 0, indicating that vertical water flux was always directed downward, towards the fractured bedrock. During winter and early spring the water potential gradient was always < 1 at all depths (except during or immediately after rainfall events), indicating that the capillarity gradient tended to impede the downward directed gravity-driven flow. Conversely, during summer the water potential gradient grew, becoming > 1 in the upper part of the profile by the end of June, indicating that capillarity summed its action to gravity, enhancing the downward flow towards the bottom of the profile. In July, the vertical gradient at the lowest depths kept on increasing, indicating leakage from the soil cover towards the underlying fractured bedrock. In the upper layer, instead, the gradient constantly decreased, becoming < 1 after the mid of July. This can be explained as an effect of the evapotranspiration from the top soil layer, which was maximum during that period.

Another feature of the field monitoring results is that in most cases the precipitation events occurring after May hardly affected suction and water content measured at any depth; conversely, soil suction was affected by rainfall events of similar characteristics occurring before May, even when the soil at the beginning of the precipitation presented similar suction values.

In particular, the seasonally variable response to precipitations seems clearly related to the seasonal variations of vegetation cover. Indeed, canopy interception capacity of precipitation is the sum of the contributions of tree foliage and understory. In woods of deciduous trees, the first contribution is obviously strongly related to the presence of leaves, with reported values of up to 6.0 mm during summer (Breuer et al., 2003), while the second is also expected to show seasonality, owing to the seasonal growth of the brushwood. Also the evapotranspiration is deeply affected by the seasonal cycle of vegetation, which sums its action to the seasonally variable climatic constraints (Herbst et al., 2008).

By coupling soil water content and suction head data measured with sensors buried at the same depths, plotted in Fig. 5, it has been possible to estimate the water retention

HESSD
10, 5799–5830, 2013

curve exhibited by the soil in the field. The experimental points clearly indicate the presence of layers with different hydraulic properties within the investigated soil profile.

3 The hydrological model

Despite the layered nature of the soil cover of the investigated slope, the proposed model attempts to simulate its hydrological behavior by means of a single homogeneous soil layer. As a consequence, the hydraulic properties of the soil constituting such a layer should be regarded as "effective" properties, useful for reliably reproducing the observed phenomena, rather than as being the actual properties of the soils belonging to the investigated profile.

Such simplified approach has been chosen for the following reasons: (i) the layered profile is extremely variable, even along the same slope, because the various layers deposited by different eruptions have been subjected to alteration, weathering, and in some cases erosion; (ii) too much information is needed for the complete hydraulic characterization of even a single soil profile at a point of a slope, hampering the practical usefulness of more sophisticated models.

Therefore, as it will be better explained in the following sections, the proposed model has been built up from the data collected during the monitoring activities. The values of soil water content and suction observed at the two instrumented locations indicate that in unsaturated conditions there are not significant differences in water potential at the same depth in different points of the slope. Thus, the gradients of all the variables along the plane parallel to the slope are negligible, and it is possible to adopt a 1-D vertical model.

As a consequence, the model consists of the classical 1-D Darcy–Buckingham motion equation along the vertical direction z, positive upward, coupled with the water mass balance equation:

$$v = -k(\theta)\frac{\partial}{\partial z}[z + \psi(\theta)] = -k(\theta)\left[1 + \frac{\partial \psi(\theta)}{\partial z}\right] \quad (1)$$

HESSD
10, 5799–5830, 2013

$$\frac{\partial \theta}{\partial t} = -\frac{\partial v}{\partial z} - q_r \tag{2}$$

In Eqs. (1) and (2) v represents the unit vertical water flux; ψ is the capillary pressure head; θ is the volumetric water content of soil; k is the hydraulic conductivity of unsaturated soil; q_r is the rate of water uptake by roots per unit volume of soil.

The two equations are combined obtaining the Richards equation with a root water uptake term:

$$\frac{d\theta}{d\psi}\frac{\partial \psi}{\partial t} = \frac{dk}{d\theta}\frac{d\theta}{d\psi}\frac{\partial \psi}{\partial z} + \frac{\partial}{\partial z}\left(k\frac{\partial \psi}{\partial z}\right) - q_r \tag{3}$$

The root water uptake q_r has been modelled by linearly distributing along the root depth, d_r, the total evapotranspiration flux (Nyambayo and Potts, 2010):

$$\begin{array}{ll} -d_r \le z \le 0 & q_r = \frac{2\kappa(\psi)\mathrm{ET_p}}{d_r}\left(1+\frac{z}{d_r}\right) \\ z < -d_r & q_r = 0 \end{array} \tag{4}$$

In Eq. (4), the potential evapotranspiration $\mathrm{ET_p}$ is evaluated by means of the Penman–Monteith equation (Shuttleworth, 1993):

$$\mathrm{ET_p} = \frac{1}{\lambda}\left[\frac{\Delta A + \rho_a c_p \frac{(1-\varphi)p_{vs}}{r_a}}{\Delta + \gamma\left(1+\frac{r_s}{r_a}\right)}\right] \tag{5}$$

In Eq. (5), λ is the latent heat of vaporization of water, ρ_a is the density of moist air, $c_p = 1.013\,\mathrm{kJ\,kg^{-1}\,°C^{-1}}$ is the specific heat of moist air, φ is air relative humidity, p_{vs} is the saturated vapor pressure, γ is the psychrometric constant, Δ is the derivative of p_{vs} with respect to air temperature, A is the available energy, r_a is the aerodynamic

HESSD
10, 5799–5830, 2013

resistance to upward vapor diffusion, r_s is the surface resistance to vapor emission by the stomata of leaves.

The quantities λ, p_{vs} and Δ depend on air temperature; γ and ρ_a depend also on atmospheric pressure. The energy available for evaporation has been assumed equal to 95 % of the total net radiation R_n:

$$R_n = S_n + L_n \quad \begin{matrix} S_n = (1-\alpha) S_0 f_c \\ L_n = \sigma f_c \left(0.27\sqrt{\varphi p_{vs}} - 0.53\right) T_a^4 \end{matrix} \quad f_c = 0.25 + 0.50\frac{n_c}{24} \tag{6}$$

In Eq. (6) $S_0 = 240\,\mathrm{W\,m^{-2}}$ represents the extraterrestrial solar radiation; $\sigma = 5.675 \times 10^{-8}\,\mathrm{W\,m^{-2}}$ is the Stefan–Boltzmann constant; f_c is the cloud cover factor, depending on the daily number of hours with clear sky, n_c; T_a is the absolute temperature of air; α is the short wave radiation reflection coefficient (albedo), depending on the vegetation type.

The following expression for the resistance r_a [$\mathrm{s\,m^{-1}}$] has been assumed:

$$r_a = \frac{\ln\left[\frac{(z_u - 0.67 h_c)}{0.123 h_c}\right]^2}{0.168 U_z} \tag{7}$$

In Eq. (7), U_z represents the speed of wind measured at elevation z_u above soil surface; h_c is vegetation height.

The function $\kappa(\psi)$ in Eq. (4), accounting for the dependence on soil water potential of the effective water uptake by roots, is here modeled as in Feddes et al. (1976):

$$\begin{matrix} \psi > \psi_1 & \kappa = 0 \\ \psi_1 \geq \psi > \psi_2 & \kappa = \frac{\psi_1 - \psi}{\psi_1 - \psi_2} \\ \psi_2 \geq \psi > \psi_3 & \kappa = 1 \\ \psi_3 \geq \psi > \psi_4 & \kappa = \frac{\psi - \psi_4}{\psi_3 - \psi_4} \\ \psi_4 \geq \psi & \kappa = 0 \end{matrix} \quad \text{with } \psi_4 < \psi_3 < \psi_2 < \psi_1 \tag{8}$$

HESSD
10, 5799–5830, 2013

In Eq. (8), ψ_1 represents the anaerobiosis point, below which the roots are supposed not to extract water from soil; ψ_2 and ψ_3 are the limits of the water potential range in which the uptake of water by roots is maximum, the first usually assumed equal to the field capacity (Nyambayo and Potts, 2010); ψ_4 is the permanent wilting point, above which plant roots are not able to extract water from soil.

The hydraulic behavior of the soil is described by introducing, in Eq. (3), appropriate expressions for the water retention curve $\psi(\theta)$ and for the hydraulic conductivity function $k(\theta)$. In the proposed model, they are described with the expressions proposed by Van Genuchten (1980) and Brooks and Corey (1964), respectively:

$$\frac{\theta - \theta_{\text{res}}}{\theta_{\text{sat}} - \theta_{\text{res}}} = \frac{1}{\left[1 + \left(\alpha_{\text{VG}}|\psi|\right)^n\right]^m} \tag{9}$$

$$k = k_{\text{sat}} \left(\frac{\theta - \theta_{\text{res}}}{\theta_{\text{sat}} - \theta_{\text{res}}}\right)^{\delta} \tag{10}$$

Therefore, for the hydraulic characterization of the unsaturated soil, the adopted expressions require the assignment of appropriate values to seven parameters: θ_{sat}, the volumetric water content of the soil at saturation; θ_{res}, the residual water content of the soil; k_{sat}, the hydraulic conductivity of the soil at saturation; α_{VG}, n, m, and δ, shape parameters related with the pore size distribution of the soil.

Equation (3) must be completed with initial and boundary conditions. The initial condition is an assigned distribution of capillary pressure head within the soil profile to be modeled. The boundary conditions have to be assigned at soil surface and at the soil-bedrock interface.

In the proposed model, the following boundary condition is written at soil surface ($z = 0$), expressing the water balance in a layer of depth dz just below the soil surface:

$$\left.\frac{\mathrm{d}\theta}{\mathrm{d}\psi}\frac{\partial\psi}{\partial t}\right|_{z=-\mathrm{d}z/2} \mathrm{d}z = i_{z=0} + k_{z=-\mathrm{d}z}\left(1 + \left.\frac{\partial\psi}{\partial z}\right|_{z=-\mathrm{d}z/2}\right) - q_{r,z=-\mathrm{d}z}\mathrm{d}z \tag{11}$$

HESSD
10, 5799–5830, 2013

In Eq. (11) $i_{z=0}$ represents the water infiltrating through the soil surface, which is:

$$\begin{array}{l}\left(R-\frac{\mathrm{d}I}{\mathrm{d}t}\right)<i_{\mathrm{p}} \Rightarrow i_{z=0}=R-\frac{\mathrm{d}I}{\mathrm{d}t} \\ \left(R-\frac{\mathrm{d}I}{\mathrm{d}t}\right)\geq i_{\mathrm{p}} \Rightarrow i_{z=0}=i_{\mathrm{p}}\end{array} \text{ with } i_{\mathrm{p}}=k_{z=0}\left(1+\left.\frac{\partial\psi}{\partial z}\right|_{z=0}\right) \quad (12)$$

In Eq. (12) R is rainfall intensity; I is the rainfall height intercepted by vegetation per unit horizontal surface; i_{p} is potential infiltration rate. The interception rate $\mathrm{d}I/\mathrm{d}t$ is assumed equal to R until the maximum interception capacity $I_{\max}$ is attained. Afterwards, $\mathrm{d}I/\mathrm{d}t$ is set to zero until rain ends.

The bottom boundary condition assumes ψ_{b}, the water potential at the soil-bedrock interface ($z = z_{\mathrm{b}}$), to follow the fluctuations of the water table of the underlying aquifer, located in the fractured calcareous rocks. Thus, in the water mass balance equation of the unit horizontal surface of the aquifer, which is schematized with a linear reservoir model, the derivative of ψ_{b} with respect to time can substitute that of the water table level $z_{\mathrm{a}} = \psi_{\mathrm{b}} + z_{\mathrm{b}}$, leading to the bottom boundary condition:

$$n_{\mathrm{a}}\frac{\mathrm{d}h_{\mathrm{a}}}{\mathrm{d}t}=i_{\mathrm{b}}-q_{\mathrm{s}}=i_{\mathrm{b}}-\frac{z_{\mathrm{a}}-z_0}{K_{\mathrm{a}}} \Rightarrow n_{\mathrm{a}}\frac{\mathrm{d}\psi_{\mathrm{b}}}{\mathrm{d}t}=k_{z=z_{\mathrm{b}}}\left(1+\left.\frac{\partial\psi}{\partial z}\right|_{z=z_{\mathrm{b}}}\right)-\frac{\psi_{\mathrm{b}}+z_{\mathrm{b}}-z_0}{K_{\mathrm{a}}} \quad (13)$$

In Eq. (13) n_{a} is the effective porosity of the calcareous fractured bedrock; i_{b} is the vertical infiltration through the soil-bedrock interface; q_{s} is the discharge of the spring draining a unit horizontal surface of the aquifer; K_{a} is the time constant of the linear reservoir model of the aquifer; z_0 is the elevation of aquifer water table corresponding to q_{s} =0.

4 Estimation of model parameters

The application of the above described model requires the assignment of values to 27 parameters, summarized in Table 1, where also the adopted value and the followed estimation method are indicated. Most of the parameters have been assigned on the

HESSD
10, 5799–5830, 2013

basis of literature and/or experimental evidence, while only 10 have been identified by means of model calibration against soil suction data provided by the monitoring activity carried out between 1 January 2011 and 20 July 2011. The identification of such parameters has been made by minimizing the sum of the squared differences between measured and estimated soil suctions at the depths of −0.60 m, −1.00 m, −1.40 m and −1.60 m, carried out by means of a genetic algorithm (Goldberg, 1989). Such an evolutionary minimum search technique allows easily to constrain the values of the unknown parameters. In fact, also for the case of parameters identified through model calibration, the unknown values have been constrained within intervals derived from field observation and/or form available experimental data.

In particular, according to information from undisturbed soil samples, θ_{sat} and θ_{res} have been constrained within the intervals [0.6, 0.75] and [0, 0.05], respectively. The other parameters defining the shape of the water retention curve of the assumed single homogeneous soil layer – namely, α_{VG}, n and m – have been constrained in such a way that the corresponding water retention curves mapped the part of the (ψ,θ) plane where the experimental data of water content and suction fell (Fig. 5). Also the parameters k_{sat} and δ defining, together with α_{VG}, n and m, the hydraulic conductivity curve of the Brooks and Corey model, have been identified through model calibration, by constraining their values within predefined intervals according to available hydraulic conductivity data measured over undisturbed samples taken at the investigated slope (Fig. 6).

The climate parameters needed for the calculation of ET_p have been obtained from the 20 yr long data set of the meteorological station of S. Croce del Sannio, located at 700 m a.s.l. around 20 km far from the slope. The wind speed at the height of 2.0m above soil surface and the number of hours with clear sky have been assumed constant and equal to their mean values (Table 1). The albedo and the vegetation height have been assigned according to the characteristics of the vegetation cover (Breuer et al., 2003). Monthly maximum and minimum values of ET_p have been evaluated by introducing monthly means of maximum and minimum air temperatures into the relevant

HESSD
10, 5799–5830, 2013

parameters of Eq. (5). Air relative humidity corresponding to maximum and minimum temperatures has been assumed 0.40 and 0.75, respectively. The daily variation of ET_p between the obtained extremes has been assumed sinusoidal, with maximum at 02:00 LT.

The other parameters related to vegetation have been considered seasonally variable. In particular, the stomatal resistance, r_s, has been assumed equal to 400 $s\,m^{-1}$ between May and September (when foliage and understory grow): the value of 625 $s\,m^{-1}$ for Italian *Castanea sativa*, reported by Breuer et al. (2003), has been reduced to account for the contribution by understory. During the other months, a value of 2800 $s\,m^{-1}$ has been assumed.

Table 2 gives the monthly minimum and maximum temperatures and the corresponding monthly mean potential evapotranspiration rates.

The maximum interception capacity by canopy, I_{max}, has been assumed equal to 1.0 mm when trees are leafless (Breuer et al., 2003; Eriksson et al., 2005), while it has been calibrated in the interval [4.0 mm, 10.0 mm] during the growing season (Table 1).

The maximum root depth, d_r, has been assumed equal to the soil cover thickness, consistently with what indicated by visual inspections of the soil profile carried out in trenches. The water potential parameters ψ_1, ψ_2, ψ_3 and ψ_4, of the root water uptake model have been assigned according to literature indications (Feddes et al., 1976; Nyambayo and Potts, 2010).

The linear reservoir model introduced to simulate the effects of the water table fluctuations upon the water potential at the interface between soil cover and bedrock requires the assignment of three parameters. The effective porosity of the fractured limestone, n_a, has been assumed equal to 0.005 according to indications found in literature for carbonate fractured rocks (Worthington and Ford, 2009). The other two parameters, identified through calibration, have been constrained in such a way to obtain that, with the typical precipitation regime, the total yearly outflow and infiltration balanced each other.

HESSD
10, 5799–5830, 2013

5 Results and discussion

Figure 7 shows the comparison between measured and simulated soil water potential during the period used for model calibration. In particular, a detail related to winter and early spring, when the trees are leafless and the understory is bare, is given in Fig. 7a, while Fig. 7b shows the obtained agreement during the vegetation growing season. Both the plots indicate that the proposed model well reproduces the observed trends.

It is worth noting that the values of the parameters allowing to achieve such results (even those which have been identified by calibration) are all in agreement with what expected either from the literature or from available information about the monitored site and the involved soil.

In particular, the water retention curve of the homogeneous soil cover simulating the behaviour of the more complex layered deposit, plotted in Fig. 5, is close to the experimental data observed in the layers deeper than 1.60 m below the soil surface, indicating that the behaviour of the layered profile is mainly determined by the finer layer. Furthermore, the hydraulic conductivity curve is in substantial agreement with the available data about unsaturated soil (Fig. 6). At saturation, the effective value results one order of magnitude larger than those provided by the measurements carried out over undisturbed saturated samples collected at the investigated slope. However, this result was expected, as in the field soil saturated hydraulic conductivity is affected by the presence of large voids, such as macropores or structural voids, which are hardly detected within small specimens in laboratory. The high value of the exponent of the Brooks and Corey hydraulic conductivity function ($\delta = 5.67$), indicating that soil texture covers a wide range of void dimensions, confirms such interpretation.

Also the identified maximum canopy interception of precipitation, referred to the period of the year when the vegetation flourishes ($I_{max} = 4.0$ mm), is in agreement with literature indications for deciduous woods (Breuer et al., 2003).

The linear reservoir model of the underlying aquifer, introduced as bottom boundary condition at the interface between soil cover and bedrock, does not mean to

HESSD
10, 5799–5830, 2013

reproduce the actual water table fluctuations, about which no experimental information is available, but rather their effects upon the water potential at the bottom. However, the identified value of the time constant K_a, multiplied times the assumed effective porosity n_a of the fractured limestone, produces a spring recession coefficient $(n_a\ K_a)^{-1} \cong 2.3 \times 10^{-1}$ days^{-1} which is in substantial agreement with those estimated for temporary or seasonal springs draining small catchments in similar hydrogeological contexts (Petrella et al., 2009).

The calibrated model has been applied to the simulation of the behaviour of the soil cover during 1999, when, on the early morning of the 16 December, a large flowslide occurred at the slope. The hourly rainfall data of the rain gauge of S. Martino Valle Caudina (BN), around 3.0 km northeast of the landslide location, have been used for the simulation. With a total yearly precipitation of 1803.6 mm, 1999 has been the fourth most rainy year since 1969. In particular, the rainfall height between March and July resulted around 230 mm higher than the average, and during 14 and 15 December, a rainfall height of 300.0 mm in 40 h was recorded.

Figure 8 reports the time history of soil water potential at various depths along the entire year 1999, as predicted by the model, together with the corresponding daily hyetograph. It looks clear how, owing to the unusually rainy spring and early summer, soil water potential, especially in the upper 0.50 m, stayed above −50.0 kPa for most of the summer. Such unusual wet conditions at the end of summer caused a fast decrease of the water potential of the entire soil layer due to the precipitations occurred in autumn (monthly rainfall heights between September and November resulted not far from the average values). Finally, the effects of the extreme rainfall event of the 14 and 15 December were enhanced by the wetness of the soil profile at the beginning of the event, when soil water potential ranged between 9.0 kPa and 25.0 kPa along the entire soil cover.

Figure 9 shows that during the rainfall event soil suction dropped down along the whole soil profile, and that, on 16 December around 05:00 LT, it was below 2.0 kPa in the upper 1.50 m, a condition never attained during all the performed simulations,

HESSD
10, 5799–5830, 2013

which, in presence of other local conditions (e.g., a higher inclination, a scarp, a road cut, etc. . . .), might lead to slope failure. This result indicates that the model is capable of adequately capturing the establishment of potential conditions of landslide triggering.

6 Conclusions

A simplified one-dimensional hydrological model of a slope covered with pyroclastic deposits is presented. The slope, with a fairly regular inclination of around 40°, is characterized by a layered cover of volcanic ashes and pumices, with an average thickness of 2.4 m, laying upon a fractured limestone bedrock.

The main simplification of the proposed model consists in the introduction of a single homogeneous soil layer in place of the layered soil profile observed at the slope. Therefore, the hydraulic characteristic curves of such single layer cannot be experimentally derived, but have been obtained through model calibration against field data. To such aim, soil water potential and volumetric water content have been measured with a time resolution of two hours at various locations and depths for more than two years. Besides, also hourly rainfall has been measured by means of a rain gauge installed at the same site. The identified parameters of the water retention curve were constrained in such a way that it resulted close to the available data of soil water content and potential observed in the field at various depths.

The data provided by field monitoring shed light also on other important features of the hydrological behaviour of the slope. In particular, water potential and volumetric water content measured in the upper soil layers indicated that the seasonal variations of the vegetation cover significantly affected infiltration and evapotranspiration processes, as well as canopy interception of precipitation: in fact, the slope is covered by deciduous chestnut woods that are leafless from October to April, and also a dense understory grows only during the late spring and summer. Therefore, the evapotranspiration has been introduced by means of a root water uptake model in which the parameters related to vegetation during the growing season have different values than from autumn

HESSD
10, 5799–5830, 2013

to early spring. Also the canopy maximum interception assumes different values in the two periods.

The field monitoring data indicated that the soil cover was always drained from the bottom, and that the highest vertical downward water potential gradient occurred during the warm and dry season (from May to September). Such behaviour can be interpreted as the effect of the fluctuations of the water table of an aquifer laying in the fractured limestone bedrock upon which the pyroclastic cover lays. Therefore, a simple linear reservoir model has been introduced as a bottom boundary condition to link the water potential at the soil-bedrock interface with the fluctuations of the water table.

Despite the simplifying assumptions made, the model counts 27 parameters. However, the physical basis of the models of the various considered hydrological processes, allows to limit to only 10 the number of parameters which have been identified through model calibration. Furthermore, also in the case of calibrated parameters, the availability of field monitoring data at high temporal resolution made possible to constrain the range of parameters variability in such a way to reduce possible problems of equifinality, leading to an approximate (but physically sound) solution of the inverse problem of parameter identification, well-posed in the Tikhonov sense (Tikhonov, 1963; Sun, 1994). In fact, an unconstrained calibration procedure could have led to overspecialization of the model for the calibration set, hampering its general validity. Instead, the calibrated model has been successfully applied to the simulation of the hydrological response of the slope to the hourly precipitations occurred during 1999, when a large flowslide occurred on the early morning of the 16 December at a location along the slope not far from the monitoring station. The results of the simulation show that the smallest soil suction profile ever observed along the entire soil width was attained just around the time when the flowslide was triggered, indicating that the model is capable of correctly predicting the potential establishment of landslide triggering conditions.

Acknowledgements. The presented results have been obtained thanks to the rainfall data kindly provided by the Centre for Meteorological Forecasting and Meteo-Hydro-Pluviometric and Landsides Monitoring of the Civil Protection Agency of Regione Campania.

HESSD
10, 5799–5830, 2013

References

Arnone, E., Noto, L. V., Lepore, C., and Bras, R. L.: Physically-based and distributed approach to analyze rainfall-triggered landslides at watershed scale, Geomorphology, 133, 121–131, 2011.

Breuer, L., Eckhardt, K., and Frede, H.-G.: Plant parameter values for models in temperate climates, Ecol. Model., 169, 237–293, 2003.

Brooks, R. H. and Corey, A. T.: Hydraulic properties of porous media, Hydrology Papers Colorado State University, 3, 1–25, 1964.

Capparelli, G. and Versace, P.: FLaIR and SUSHI: two mathematical models for early warning of landslides induced by rainfall, Landslides, 8, 67–79, 2010.

Cascini, L., Cuomo, S., and Guida, D.: Typical source areas of May 1998 flow-like mass movements in the Campania region, Southern Italy, Eng. Geol., 96, 107–125, 2008.

Celico, F., Petrella, E., and Celico, P.: Hydrogeological behaviour of some fault zones in a carbonate aquifer of Southern Italy: an experimentally based model, Terra Nova, 18, 308–313, 2006.

Crosta, G. B. and Dal Negro, P.: Observations and modelling of soil slip-debris flow initiation processes in pyroclastic deposits: the Sarno 1998 event, Nat. Hazards Earth Syst. Sci., 3, 53–69, doi:10.5194/nhess-3-53-2003, 2003.

Di Crescenzo, G. and Santo, A.: Debris slides–rapid earth flows in the carbonate massifs of the Campania region (Southern Italy): morphological and morphometric data for evaluating triggering susceptibility, Geomorphology, 66, 255–276, 2005.

Eriksson, H., Eklundh, L., Hall, K., and Lindroth, A.: Estimating LAI in deciduous forest stands, Agr. Forest Meteorol., 129, 27–37, 2005.

Feddes, R. A., Kowalik, P., Kolinska-Malinka, K., and Zaradny, H.: Simulation of field water uptake by plants using a soil water dependent root extraction function, J. Hydrol., 31, 13–26, 1976.

Goldberg, D. E.: Genetic Algorithms in Search, Optimization and Machine Learning, Addison-Wesley, Reading, MA, 1989.

Greco, R., Guida, A., Damiano, E., and Olivares, L.: Soil water content and suction monitoring in model slopes for shallow flowslides early warning applications, Phys. Chem. Earth., 35, 127–136, 2010.

HESSD
10, 5799–5830, 2013

Guadagno, F. M., Forte, R., Revellino, P., Fiorillo, F., and Focareta, M.: Some aspects of the initiation of debris avalanches in the Campania region: the role of morphological slope discontinuities and the development of failure, Geomorphology, 66, 237–254, 2005.

Guzzetti, F., Peruccacci, S., Rossi, M., and Stark, C. P.: Rainfall thresholds for the initiation of landslides in central and southern Europe, Meteorol. Atmos. Phys., 98, 239–267, 2007.

Herbst, M., Rosier, P. T. W., McNeil, D. D., Harding, R. J., and Gowing, D.: Seasonal variability of interception evaporation from the canopy of a mixed deciduous forest, Agr. Forest Meteorol., 148, 1655–1667, 2008.

Ivanov, V., Bras, R. L., and Vivoni, E. R.: Vegetation-hydrology dynamics in complex terrain of semiarid areas: II. energy–water controls of vegetation spatio-temporal dynamics and topographic niches of favorability, Water Resour. Res., 44, WR005588, doi:10.1029/2006WR005595, 2008a.

Ivanov, V. Y., Bras, R. L., and Vivoni, E. R.: Vegetation-hydrology dynamics in complex terrain of semiarid areas: I a mechanistic approach to modeling dynamic feedbacks, Water Resour. Res., 44, WR005595, doi:10.1029/2006WR005588, 2008b.

Montgomery, D. R. and Dietrich, W. E.: A physically based model for the topographic control on shallow landsliding, Water Resour. Res., 30, 1153–1171, 1994.

Muyzlo, A., Llorens, P., Valente, F., Keizer, J. J., Domingo, F., and Gash, J. H. C.: A review of rainfall interception modelling, J. Hydrol., 370, 191–206, 2009.

Netti, N., Damiano, E., Greco, R., Olivares, L., Savastano, V., and Mercogliano, P.: Natural hazard risk management: a multidisciplinary approach to define a decision support system for shallow rainfall-induced landslides, The Open Hydrology Journal, 6, 97–111, 2012.

Nyambayo, V. P. and Potts, D. M.: Numerical simulation of evapotranspiration using a root water uptake model, Comput. Geotech., 37, 175–186, 2010.

Olivares, L. and Picarelli, L.: Susceptibility of loose pyroclastic soils to static liquefaction: some preliminary data, in: Proceedings of International Conference on Landslides – Causes, Impacts and Countermeasures, Vol. 1, Davos, Switzerland, 75–85, 2001.

Petrella, E., Capuano, P., and Celico, F.: Unusual behaviour of epikarst in the Acqua dei Faggi carbonate aquifer (Southern Italy), Terra Nova, 19, 82–88, 2007.

Petrella, E., Capuano, P., Carcione, M., and Celico, F.: A high-altitude temporary spring in a compartmentalized carbonate aquifer: the role of low-permeability faults and karst conduits, Hydrol. Process., 23, 3354–3364, 2009.

HESSD
10, 5799–5830, 2013

Regalado, C. M., Munoz Carena, R., Socorro, A. R., and Hernandez Moreno, J. M.: Time domain reflectometry models as a tool to understand the dielectric response of volcanic soils, Geoderma, 117, 313–330, 2003.
Rolandi, G., Bellucci, F., Heizler, M. T., Belkin, H. E., and De Vivo, B.: Tectonic controls on the genesis of ignimbrites from the Campanian Volcanic Zone, southern Italy, Miner. Petrol., 79, 3–31, 2003.
Rosso, R., Rulli, M. C., and Vannucchi, G.: A physically based model for the hydrologic control on shallow landsliding, Water Resour. Res., 42, W06410, doi:10.1029/2005WR004369, 2006.
Shuttleworth, W. J.: Evaporation, in: Handbook of Hydrology, edited by: Maidment, D., McGraw-Hill inc., New York, 4.1–4.40, 1993.
Sun, N.-Z.: Inverse Problems in Groundwater Modeling, Kluwer Academic Publishers, Dordrecht, 1994.
Tikhonov, A. N.: Solution of ill-posed problems and the regularization method, Soviet Mathematics Doklady, 4, 1035–1038, 1963.
van Genuchten, M. T.: A closed-form equation for predicting the hydraulic conductivity of unsaturated soil, Soil. Sci. Soc. Am. J., 44, 615–628, 1980.
Versace, P., Sirangelo, B., and Capparelli, G.: Forewarning model of landslides triggered by rainfall, in: Proceedings of 3rd International Conference on Debris-flow Hazards Mitigation: Mechanics, Prediction and Assessment, Vol. 2, Davos, Switzerland, 1233–1244, 2003.
Worthington, S. R. H. and Ford, D. C.: Self-organized permeability in carbonate aquifers, Ground Water, 47, 326–336, 2009.

HESSD
10, 5799–5830, 2013

Table 1. Summary of model parameters.

Model parameter		Estimation method	Lower limit	Upper limit	Adopted value
Soil hydraulic characteristics	Saturated water content θ_{sat}	calibrated	0.6	0.75	0.749
	Residual water content θ_{res}		0.0	0.05	0.008
	van Genuchten parameter α_{VG} (m^{-1})		8.0	15.0	11.78
	van Genuchten parameter m		0.5	1.1	0.676
	van Genuchten parameter n		0.7	1.2	0.683
	Saturated hydraulic conductivity k_{sat} ($m\,s^{-1}$)		2.8×10^{-6}	1.7×10^{-4}	8.04×10^{-5}
	Brooks and Corey exponent δ		3.0	6.0	5.67
Potential evapo-transpiration	Winter stomatal resistance r_a (sm^{-1})	assigned (Breuer et al.,	–	–	2800
	Summer stomatal resistance r_a (sm^{-1})	2003)	–	–	400
	Albedo α		–	–	0.25
	Vegetation height h_c (m)	assigned (visual	–	–	15.0
	Wind speed U_z ($m\,s^{-1}$)	inspection)	–	–	1.0
	Daily hours with clear sky n_c		–	–	19
	Monthly max temperature T_{max} (°C)	assigned (mean of	–	–	see Table 2
	Monthly min temperature T_{min} (°C)	meteorological data)	–	–	see Table 2
	Maximum air relative humidity φ_{max}		–	–	0.75
	Minimum air relative humidity φ_{min}		–	–	0.40
Canopy interception	Winter maximum interception capacity I_{max} (mm)	assigned (Breuer et al., 2003)	–	–	1.0
	Summer maximum interception capacity I_{max} (mm)	calibrated	4.0	10.0	4.0
Root water uptake	Maximum root depth d_r (m)	assigned (visual inspection)	–	–	2.4
	Anaerobiosis point ψ_1 (m)	assigned (Feddes et al., 1976)	–	–	0.0
	Field capacity ψ_2 (m)	assigned (Nyambayo and Potts, 2010)	–	–	0.5
	Water potential ψ_3 (m)	assigned (Feddes et al., 1976)	–	–	15.0
	Permanent wilting point ψ_4 (m)		–	–	150.0
Aquifer linear reservoir	Spring outlet elevation z_q (m)	calibrated	5.0	10.0	7.97
	Aquifer effective porosity n_a	assigned (Worthington and Ford, 2009)	–	–	0.005
	Aquifer time constant K_a (days)	calibrated	700	1300	871

HESSD
10, 5799–5830, 2013

Table 2. Monthly mean climatic characteristics of Cervinara and corresponding estimated potential evapotranspiration fluxes.

Month	Mean monthly rainfall height [mm]	Mean monthly minimum temperature [°C]	Mean monthly maximum temperature [°C]	Mean monthly minimum potential evapotranpiration rate [mm day^{-1}]	Mean monthly maximum potential evapotranpiration rate [mm day^{-1}]
Jan	135	1.3	6.5	0.05	0.14
Feb	150	1.1	6.8	0.05	0.15
Mar	121	2.9	9.6	0.05	0.18
Apr	109	5.5	12.9	0.06	0.22
May	74	10.0	18.3	0.55	1.93
Jun	46	13.5	22.2	0.69	2.40
Jul	32	16.3	25.9	0.82	2.94
Aug	47	16.2	25.7	0.81	2.91
Sep	80	13.5	22.2	0.69	2.40
Oct	115	9.9	17.4	0.08	0.28
Nov	187	5.2	11.3	0.06	0.19
Dec	163	2.7	7.9	0.05	0.16

HESSD
10, 5799–5830, 2013

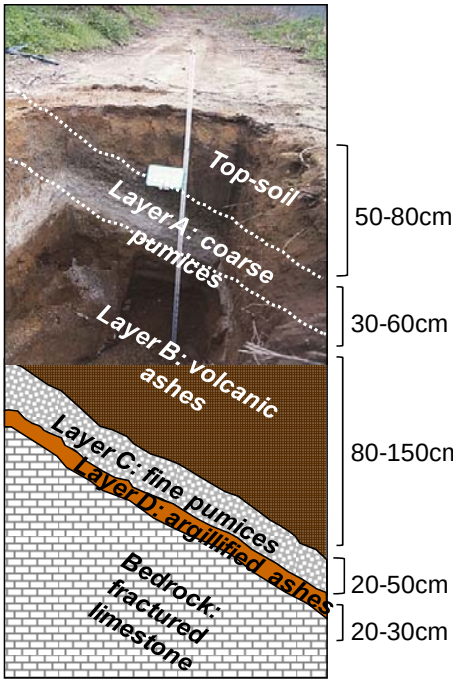

Fig. 1. Example of the layered profile of the soil cover of the slope of Cervinara.

HESSD
10, 5799–5830, 2013

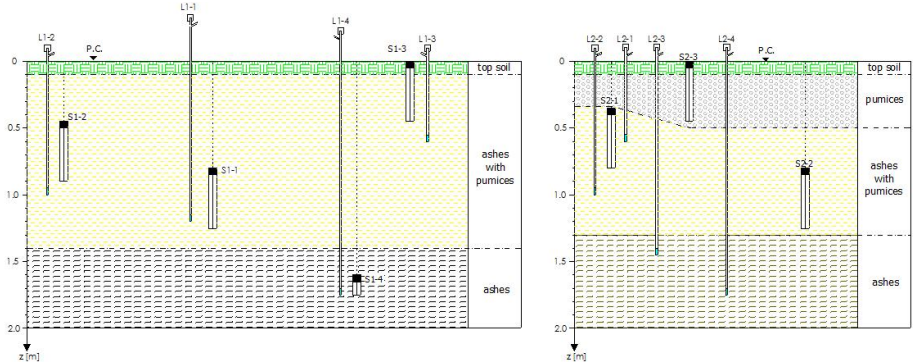

Fig. 2. Sketch of the instruments installed at the field monitoring station: L = tensiometers; S = TDR probes (the sketched vertical section is orthogonal to the direction of maximum inclination of the slope).

HESSD
10, 5799–5830, 2013

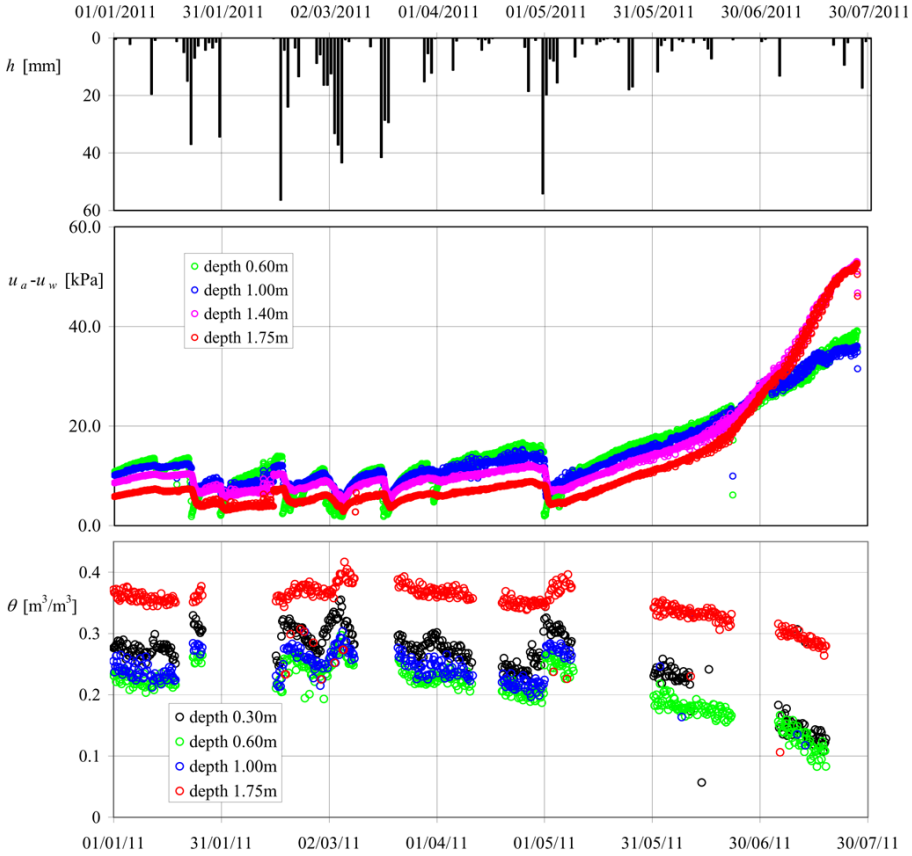

Fig. 3. Field monitoring data observed at various depths between 1 January 2011 and 20 July 2011. From top to bottom: daily rainfall height; soil suction; soil volumetric water content.

HESSD
10, 5799–5830, 2013

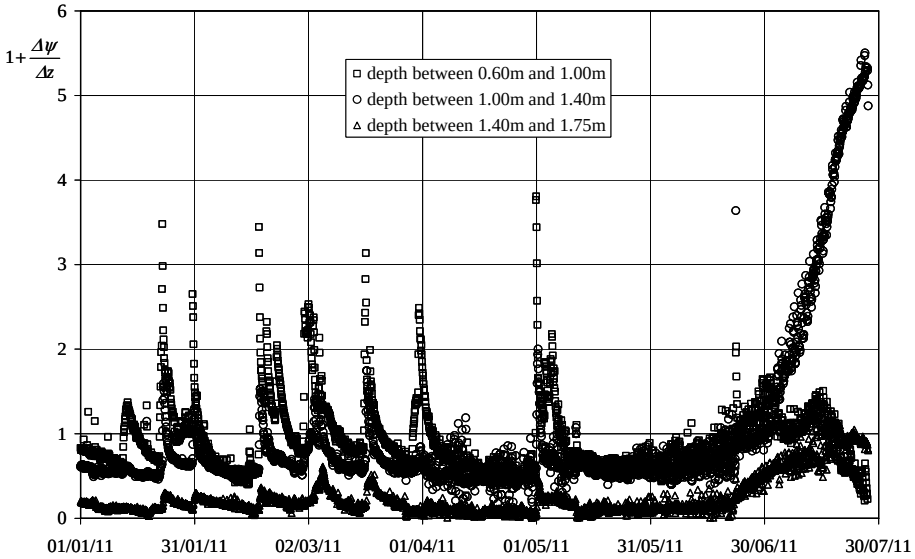

Fig. 4. Soil water potential vertical gradients estimated from field measurements.

HESSD
10, 5799–5830, 2013

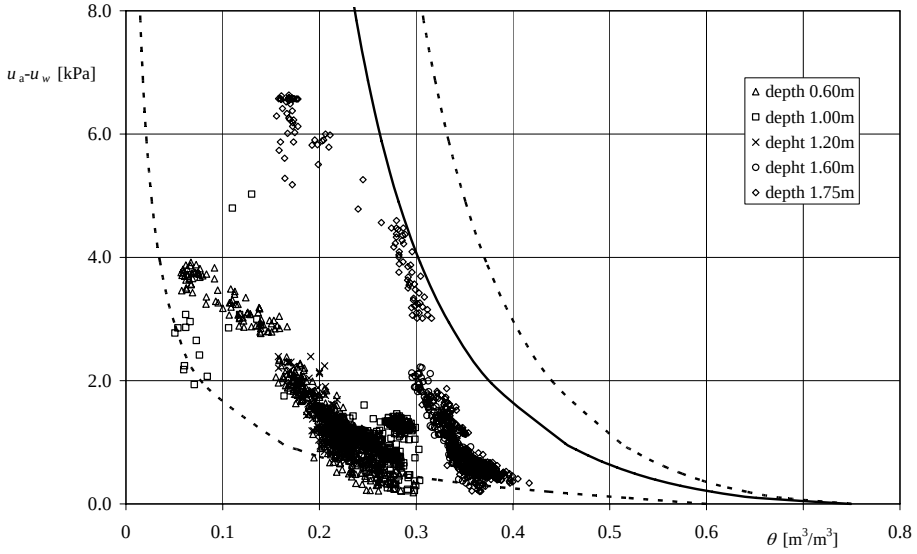

Fig. 5. Water retention of the investigated soil: dots represent field experimental data at various depths; the bold line is the calibrated water retention curve of the assumed single homogeneous layer; the dashed lines represent the limits of the range of water retention curves considered in the calibration procedure.

HESSD
10, 5799–5830, 2013

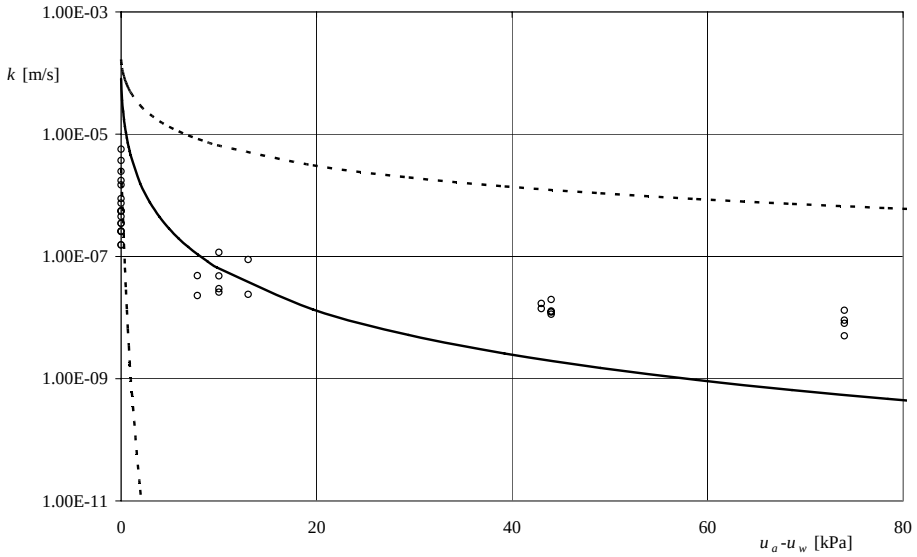

Fig. 6. Hydraulic conductivity of the investigated soil: dots represent laboratory experimental data; the bold line is the calibrated hydraulic conductivity curve of the assumed single homogeneous layer; the dashed lines represent the limits of the range of hydraulic conductivity curves considered in the calibration procedure.

HESSD
10, 5799–5830, 2013

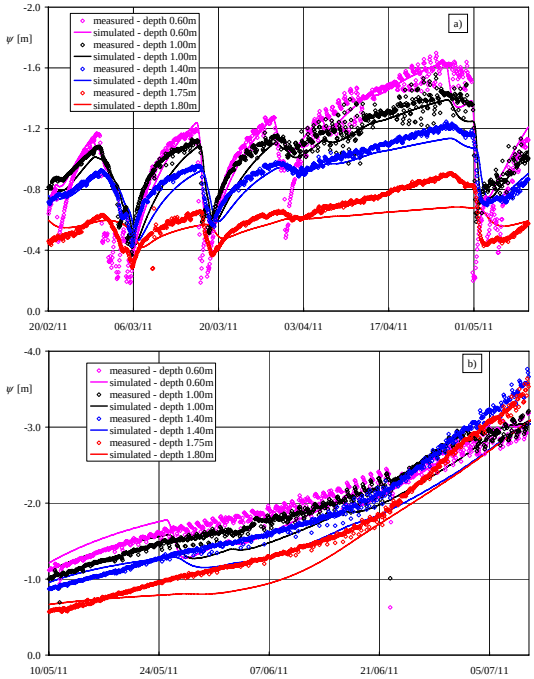

Fig. 7. Comparison between simulated and observed soil water potential at various depths with leafless trees and low-developed understory (above), and during the vegetation growing period (below).

HESSD
10, 5799–5830, 2013

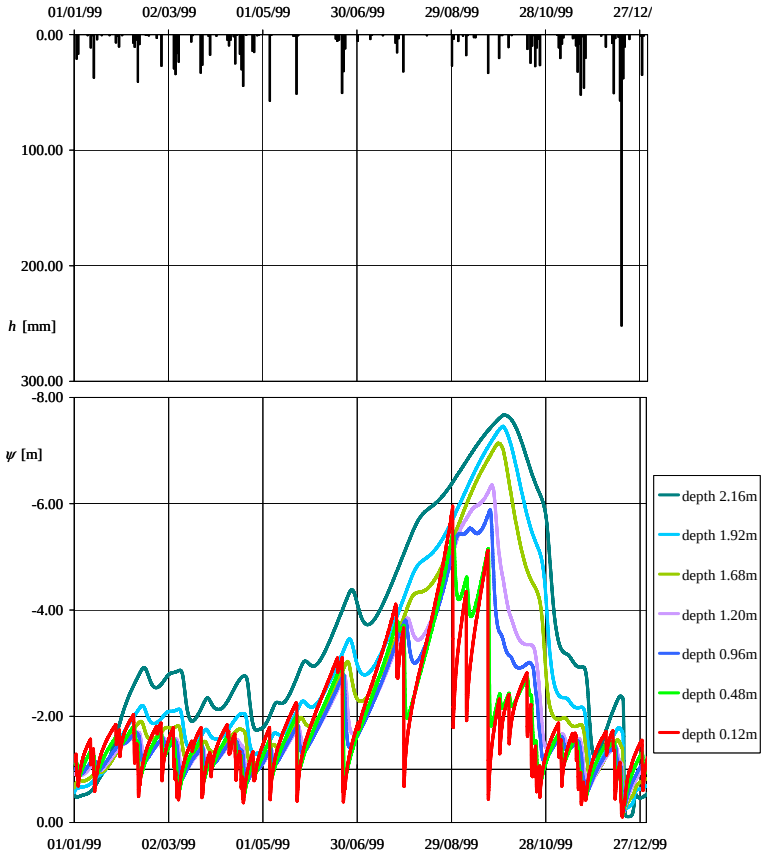

Fig. 8. Daily hyetograph (above) and simulated soil water potential at various depths (below) during 1999.

HESSD
10, 5799–5830, 2013

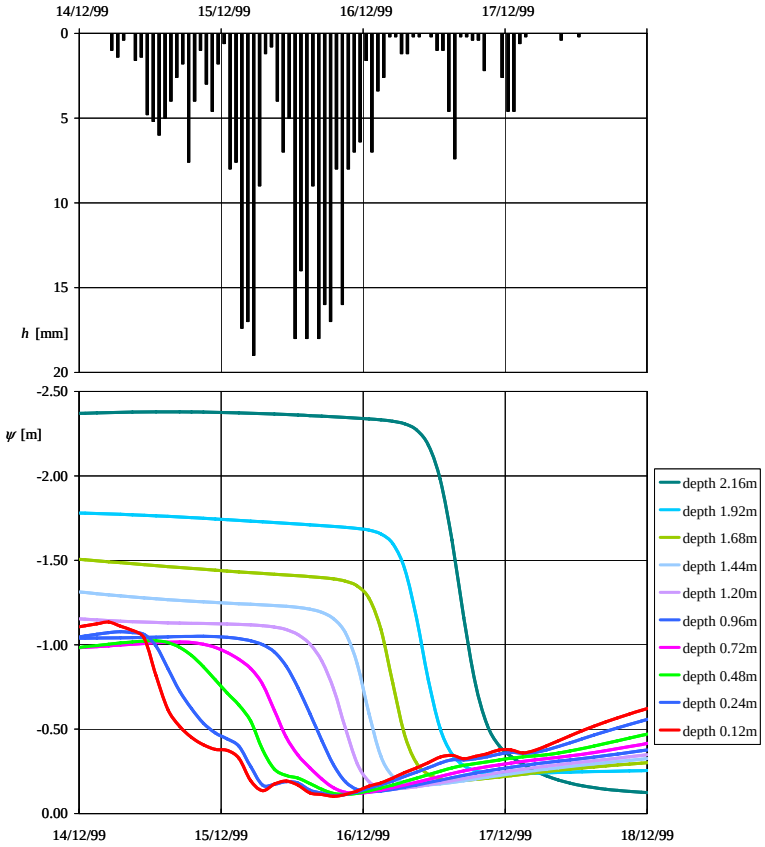

Fig. 9. Hourly hyetograph (above) and simulated soil water potential at various depths (below) during the rainfall event of 14 to 16 December, when a flowslide was triggered on the early morning of 16 December.

HESSD
10, 5799–5830, 2013